PERGAMON

International Journal of Heat and Mass Transfer 43 (2000) 3725–3734

International Journal of HEAT and MASS TRANSFER

www.elsevier.com/locate/ijhmt

# Statistical modelling of mass transfer in turbulent two-phase dispersed flows — 2. Calculation results

I.V. Derevich

*Moscow State University of Environmental Engineering, 21/4 Staray Basmannaya Street, 107884 Moscow, Russia*

**Abstract**

A closed numerical model of hydrodynamics and mass transfer of dispersed particles impurity in a turbulent two-phase flow in vertical pipe is developed. Within the framework of two-equation model of turbulence (turbulent energy–turbulent dissipation rate), particles deposition velocity, intensity of dispersed phase chaotic motion and average velocity slip between dispersed and carrying phases are calculated. The theoretical results are compared with the experimental data. 

## 1. Introduction

This paper is devoted to developing the description of hydrodynamics and mass transfer in a turbulent two-phase flow in Eulerian variables. In the first part of the work [1], the theoretical model of turbulent flow with an impurity of particles of the spherical shape in absence of particle–particle collisions was presented. On the basis of the method of probability density function (PDF), a closed system of balance equations of concentration, momentum and intensity of a chaotic motion of the dispersed phase in nonhomogeneous flow was presented. Taking into account the exchange of impulse between colliding particles and surface and particles absorption on the surface, boundary conditions were obtained.

In this paper, we present results of careful testing of the theoretical model [1] for a turbulent two-phase flow in vertical pipes with regard to particles deposition on walls. On the basis of two-equation ($E$–$\varepsilon$) turbulence model used in engineering applications, a closed numerical model for calculation of hydrodynamics and dispersed phase mass transfer in vertical pipes is developed. The model calculations are compared with experimental data and results of direct numerical simulations obtained by other authors.

## 2. Balance equations of a two-phase flow in a pipe

### 2.1. Dispersed phase motion equations in a pipe

Stationary, fully-developed turbulent flow in a vertical pipe is examined. The balance equation of the dispersed phase momentum in axial direction rewritten from Part 1 [1] is

$$V_r \frac{dV_x}{dr} + \frac{1}{rC}\frac{d}{dr}(rC\langle v_x v_r\rangle) = \frac{U_x + V_s - V_x}{\tau} \quad (1)$$

In Eq. (1), we ignore the term proportional to production of dispersed phase gradients of velocity and concentration.

The second moment of particles velocity fluctuations in Eq. (1) represents turbulent stresses in the dispersed phase, arising as a result of particles involving in tur-

*E-mail address:* igor@derevich.msk.ru (I.V. Derevich).

0017-9310/00/$ - see front matter 
PII: S0017-9310(00)00039-9

**Nomenclature**

| | |
|---|---|
| $C$, $C_m$, $C_c$, $C_w$ | dispersed phase concentration, mean concentration, concentration on the pipe axis and on the pipe wall |
| $C_D$ | drag coefficient for particles |
| $c_\mu$, $c_{\varepsilon 1}$, $c_{\varepsilon 2}$, $c_{\varepsilon 3}$ | constants for turbulence model |
| $d_p$ | particle diameter (m) |
| $D_p$ | coefficient of turbulent diffusion of particles ($m^2\ s^{-1}$) |
| $E$ | mean turbulent energy of fluid phase ($m^2\ s^{-1}$) |
| $f_1, f_2, f_m$ | correction functions |
| $g$ | particles response function |
| $J$ | particles deposition velocity ($m\ s^{-1}$) |
| $k_n$, $k_t$ | coefficients of impulse restitution in normal and axial directions |
| $L_E$ | Eulerian spatial macroscale (m) |
| $q$ | particles response function |
| $r$ | radial coordinate (m) |
| $R$ | radius of a pipe (m) |
| $Re$ | flow Reynolds number, $U_m 2R/\nu_g$ |
| $Re_p$ | particle Reynolds number, $Wd_p/\nu_g$ |
| $T_E$, $T_E^o$, $T_W$ | Eulerian time macroscales in the hole flow, in the flow core and in viscous sublayer (s) |
| $T_L$ | Lagrangian time macroscale (s) |
| $U_m$ | mean velocity of the flow ($m\ s^{-1}$) |
| $U_x$ | axial velocity of the flow ($m\ s^{-1}$) |
| $u_x$, $u_r$ | velocity fluctuations in axial and radial directions ($m\ s^{-1}$) |
| $u$ | amplitude of turbulent velocity of fluid phase ($m\ s^{-1}$) |
| $V_{mig}$ | turbophoretic velocity ($m\ s^{-1}$) |
| $V_x$, $V_r$ | components of averaged dispersed phase velocity in axial and radial directions ($m\ s^{-1}$) |
| $V_s$ | particles sedimentation velocity due to mass forces ($m\ s^{-1}$) |
| $v_x$, $v_r$ | fluctuations of dispersed phase velocity in axial and radial directions ($m\ s^{-1}$) |
| $y$ | dimensionless coordinate normal to the wall, $1 - r/R$ |
| $W$ | modulus of relative velocity between continuous and dispersed phase ($m\ s^{-1}$) |
| *Greek symbols* | |
| $\gamma$ | parameter associated with internal turbulent structure, $uT_L/L_E$ |
| $\beta$ | ratio of Lagrangian and Eulerian time macroscales |
| $\beta_E$ | constant in the expression for turbulent time scale |
| $\varepsilon$ | turbulent dissipation rate ($m^2\ s^{-3}$) |
| $\nu_g$ | kinematics viscosity coefficient of fluid ($m^2\ s^{-1}$) |
| $\chi$ | absorption coefficient |
| $\rho_p$, $\rho_g$ | particles and fluid densities ($kg\ m^{-3}$) |
| $\tau$ | particle dynamic relaxation time (s) |
| *Subscript* | |
| $+$ | denotes the dimensionless variables in dynamic universal units |

bulent motion

$$\langle v_x v_r\rangle = q\langle u_x u_r\rangle - \frac{\tau}{2}\langle v_r^2\rangle\frac{\partial V_x}{\partial r} \tag{2}$$

The intensity of a chaotic motion of the dispersed phase in radial direction is calculated from the balance equation [1]

$$V_r\frac{d\langle v_r^2\rangle}{dr} + \frac{1}{rC}\frac{d}{dr}\left(rC\langle v_r^3\rangle\right) = \frac{2}{\tau}\left(q\langle u_r^2\rangle - \langle v_r^2\rangle\right) \tag{3}$$

$\langle u_i^2\rangle$ is intensity of turbulent velocity fluctuations of a carrying phase in $i$th direction.

The third correlation in Eq. (3) describes the turbulent transfer of dispersed phase chaotic motion intensity in radial direction [1]

$$\langle v_r^3\rangle = -\tau\langle v_r^2\rangle\frac{d\langle v_r^2\rangle}{dr} \tag{4}$$

The equation for intensity of the dispersed phase turbulent velocity in axial direction have the form [1]

$$V_r\frac{d\langle v_x^2\rangle}{dr} + \frac{1}{rC}\frac{d}{dr}\left(rC\langle v_x^2 v_r\rangle\right) + \langle v_x v_r\rangle\frac{\partial\langle V_x\rangle}{\partial r} = \frac{2}{\tau}\left(q\langle u_x^2\rangle - \langle v_x^2\rangle\right) \tag{5}$$

The third turbulent velocity correlation in Eq. (5) represents the turbulent transfer of chaotic particles motion in axial direction [1]

$$\langle v_x^2 v_r\rangle = -\frac{\tau}{3}\langle v_r^2\rangle\frac{\partial\langle v_x^2\rangle}{\partial r} \tag{6}$$

The dynamic relaxation time of particles in Eqs. (1)–(6) depends on the relative averaged velocity between dispersed and carrying phases

$$\tau = \frac{4}{3}\frac{\rho_s}{\rho_g}\frac{d_p^2}{\nu_g}\frac{1}{Re_p C_D}, \quad Re_p = Wd_p/\nu_g, \quad W = |V - U|$$

$$C_D = \frac{24}{Re_p}\left(1 + 0.179Re_p^{0.5} + 0.013Re_p\right)$$

Balance of the dispersed phase concentration in the pipe cross-section is regulated by particles deposition on the pipe wall and is described by the following equations [1]

$$CV_r = \underbrace{-C\tau\frac{1}{r}\frac{d}{dr}\left(r\langle v_r^2\rangle\right)}_{I} - \underbrace{CD_p\frac{d\ln C}{dr}}_{II} = \frac{r}{R}JC_m \tag{7}$$

$$C_m = \frac{2}{R^2}\int_0^R dr\, rC(r)$$

where $C_m$ is mean concentration of particles in the pipe cross-section.

The radial component of average velocity of the dispersed phase in Eq. (7) is sum of the turbophoretic velocity (I), connected with nonhomogeneity of dispersed phase turbulent energy, and diffusion velocity of particles, caused by a gradient of impurity concentration (II). The derivation of Eq. (7) is given in Appendix A.

The coefficient of particles turbulent diffusion in Eq. (7) is associated with the chaotic motion of particles and their random movement, together with the powerful turbulent eddies of the carrying phase [1]

$$D_p = \tau\left(\langle v_r^2\rangle + g\langle u_r^2\rangle\right) \tag{8}$$

The particles response functions $g$, $q$ in Eqs. (2), (3), (5) and (8) depend on the contact time of particles with powerful turbulent fluid eddies. These functions are calculated in conformity with results of Derevich [1].

The boundary conditions for balance equations (1), (3), (5) and (7) were designed in [1] under the assumption that the particles reflected from the wall have a velocity lower than that before the collision. The axial and radial velocities of particles before and after their collisions against the wall were related to each other by the coefficients of restitution $k_n$, $k_t$. Moreover, in [1], the probability of particles absorption on the wall, described by absorption coefficient $\chi$, was included. At $\chi = 0$, all particles touching the wall leave the flow; at $\chi = 1$, the particles are not absorbed on the surface.

The system of boundary conditions for concentration, averaged velocity and intensity of radial and axial chaotic motion of dispersed phase on the pipe wall ($r = R$) consists of the following relations [1]

$$\left[\frac{1-\chi}{1+\chi}\left(\frac{2}{\pi}\langle v_r^2\rangle\right)^{1/2} - V_r\right] = 0 \tag{9}$$

$$\left[\frac{1-\chi k_t}{1+\chi k_t}\left(\frac{2}{\pi}\langle v_r^2\rangle\right)^{1/2} - V_r\right]V_x = -\frac{\tau}{2}\langle v_r^2\rangle\frac{\partial V_x}{\partial r} \tag{10}$$

$$\left[\frac{1-\chi k_n^2}{1+\chi k_n^2}2\left(\frac{2}{\pi}\langle v_r^2\rangle\right)^{1/2} - V_r\right]\langle v_r^2\rangle = -\tau\langle v_r^2\rangle\frac{\partial\langle v_r^2\rangle}{\partial r} \tag{11}$$

$$\left[\frac{1-\chi k_t^2}{1-\chi k_t^2}\left(\frac{2}{\pi}\langle v_r^2\rangle\right)^{1/2} - \langle V_r\rangle\right]\langle v_x^2\rangle = -\frac{\tau}{3}\langle v_r^2\rangle\frac{\partial\langle v_x^2\rangle}{\partial r} \tag{12}$$

In the present study, we consider only the turbulent effect of fluid on particles but we ignore modification in the carrying phase turbulence due to the presence of particles.

### 2.2. Turbulent fluid flow equations in a pipe

The conventional ($E$–$\epsilon$) model, for example [2], includes the following equations for the turbulent flow, which are written for a stabilised flow:

1. Equation for axial velocity of the carrying phase

$$-\frac{1}{\rho_g}\frac{\partial P}{\partial x} + \frac{1}{r}\frac{\partial}{\partial r}\left[r(\nu_g + \nu_t)\frac{\partial U_x}{\partial r}\right] = 0 \tag{13}$$

where $P$ is pressure in continuous phase.

Turbulent stress and turbulent viscosity in continuous phase are given by

$$\langle u_x u_r\rangle = -\nu_t\frac{\partial U_x}{\partial r}, \quad \nu_t = c_\mu f_\mu E^2/\epsilon \tag{14}$$

2. Equation for the mean turbulent energy of the carrying phase

$$\frac{1}{r}\frac{\partial}{\partial r}\left[r(\nu_g + \nu_t)\frac{\partial E}{\partial r}\right] + \nu_t\left(\frac{\partial U_x}{\partial r}\right)^2 - \epsilon = 0 \tag{15}$$

3. Equation for the mean turbulent energy dissipation rate

$$\frac{1}{r}\frac{\partial}{\partial r}\left[r\left(\nu_g + \frac{\nu_t}{c_{\epsilon 3}}\right)\frac{\partial\epsilon}{\partial r}\right] + \nu_t c_{\epsilon 1} f_1\frac{\epsilon}{E}\left(\frac{\partial U_x}{\partial r}\right)^2 - c_{\epsilon 2} f_2\frac{\epsilon^2}{E} = 0 \tag{16}$$

The correction functions $f_1$, $f_2$ and $f_\mu$, as well as the constants $c_\mu$, $c_{\epsilon 1}$, $c_{\epsilon 2}$, $c_{\epsilon 3}$ of the ($E$–$\epsilon$) model equations,

are taken from [2]. The Eulerian time macroscale of turbulence in the flow core is determined from the relation

$$T_{\mathrm{E}}^{\mathrm{o}} = \beta_{\mathrm{E}} E/\epsilon$$

where the constant $\beta_{\mathrm{E}} \approx 0.22$ [3].

Near the wall, the time scale of turbulence in dimensionless variables is approximated with regard to the macroscale of turbulent bursts in the viscous sublayer [4]

$$T_{\mathrm{E}+} = \sqrt{\left(T_{E+}^{\mathrm{o}}\right)^2 + \left(T_{w+}\right)^2}, \quad T_{w+} \approx 10$$

where index "+" here and further marks dimensionless parameters in universal dynamic variables.

The radial component of velocity fluctuation of the carrying phase associates with turbulent viscosity

$$\nu_{\mathrm{t}} = \langle u_{\mathrm{r}}^2 \rangle T_{\mathrm{E}} \tag{17}$$

The spatial macroscale of turbulence can be determined using the Prandtl hypothesis

$$\nu_{\mathrm{t}} = L_{\mathrm{E}} \langle u_{\mathrm{r}}^2 \rangle^{1/2}$$

We approximate the intensity of carrying phase velocity fluctuations in axial direction as $\langle u_{\mathrm{x}}^2 \rangle \approx 1.3E$.

On the pipe axis for Eqs. (1), (3) and (5), Eqs. (13), (15) and (16) are used as conditions of symmetry. On the pipe wall, the fluid phase is set to zero value for the averaged velocity and for the turbulent energy, and for a gradient of the turbulent dissipation rate.

## 3. Analytical expression for deposition velocity of inertial particles

Here, we study a flow with dispersed impurity of rather inertial particles, the time of dynamic relaxation of which exceeds the time macroscale of turbulence $\tau > T_{\mathrm{E}}$. For sufficiently inertial particles, the profile of turbulent particles energy is more flat across the pipe section. But the turbulent particles diffusivity without average velocity slip between phases weakly depends on the particles inertia (as an example, see [6]). So, in the equation for dispersed phase concentration, Eq. (7), it is possible to neglect the turbophoretic velocity of particles. Without taking into account the particles energy gradient, the equation for dispersed phase concentration appears as

$$CV_{\mathrm{r}} = -D_{\mathrm{p}} \frac{\mathrm{d}C}{\mathrm{d}r} = \frac{r}{R} J C_{\mathrm{m}} \tag{18}$$

Eq. (18) has the analytical solution for computation of the distribution of concentration of the impurity on the pipe cross-section and the rate of particles turbulent deposition

$$\frac{C}{C_{\mathrm{w}}} = 1 + \frac{RJ^{\mathrm{o}}}{2D_{\mathrm{p}}}\left(1 - \frac{r^2}{R^2}\right) \tag{19}$$

$$\frac{C_{\mathrm{m}}}{C_{\mathrm{w}}} = 1 + \frac{1}{4}\frac{J^{\mathrm{o}}R}{D_{\mathrm{p}}}, \quad J^{\mathrm{o}} = \frac{1-\chi}{1+\chi}\left(\frac{2}{\pi}\langle v_r^2 \rangle\right)^{1/2}$$

$$J = J^{\mathrm{o}}\frac{C_{\mathrm{w}}}{C_{\mathrm{m}}} = \left[\frac{1-\chi}{1-\chi}\left(\frac{2}{\pi}\langle v_{\mathrm{r}}^2 \rangle\right)^{1/2}\right]\left[1 + \frac{1}{4}\frac{R}{D_{\mathrm{p}}}\frac{1-\chi}{1-\chi}\left(\frac{2}{\pi}\langle v_{\mathrm{r}}^2 \rangle\right)^{1/2}\right]^{-1} \tag{20}$$

where $C_{\mathrm{w}}$ is concentration on the pipe wall.

For inertial particles, $\tau > T_{\mathrm{E}}$ = the intensity of dispersed phase chaotic motion is expressed through turbulent energy of carrying phase in radial direction in accordance with the following relations [1,5]

$$\langle v_{\mathrm{r}}^2 \rangle \approx \langle u_{\mathrm{r}}^2 \rangle \frac{T_{\mathrm{E}}}{\tau}, \quad T_{\mathrm{E}} = \frac{L_{\mathrm{E}}}{\langle u_{\mathrm{r}}^2 \rangle^{1/2}}, \quad L_{\mathrm{E}} = aR, \quad \langle u_{\mathrm{r}}^2 \rangle \approx u_+^2 \tag{21}$$

where $u_+$ is the dynamic (friction) velocity of the fluid flow, and $a \approx 0.14$.

The coefficient of turbulent diffusion of particles is approximated according to [6]

$$D_{\mathrm{p}} \approx bRu_+, \quad b \approx 0.074 \tag{22}$$

The following formulae are derived from Eqs. (19)–(22) to evaluate the concentration profile of the dispersed phase and the dimensionless particles deposition rate:

$$A = \frac{1-\chi}{1+\chi}\left(\Gamma\frac{R_+}{\tau_+}\right)^{1/2}, \quad \Gamma = 2a/\pi$$

$$\frac{C}{C_{\mathrm{w}}} = \left(1 + \frac{A}{2b}\right)^{-1}\left[1 + \frac{A}{2b}\left(1 - \frac{r^2}{R^2}\right)\right] \tag{23}$$

$$J_+ = \frac{J}{u_+} = \frac{A}{1 + A/(4b)} \tag{24}$$

The maximum deposition velocity is reached in Eq. (24) for absorbing wall $\chi = 0$ at $\tau_+ \ll aR_+$ and its value is equal to $J_+ = 4b \approx 0.3$. For particles with small inertia, the dispersed phase concentration on the absorbing wall decreases to zero.

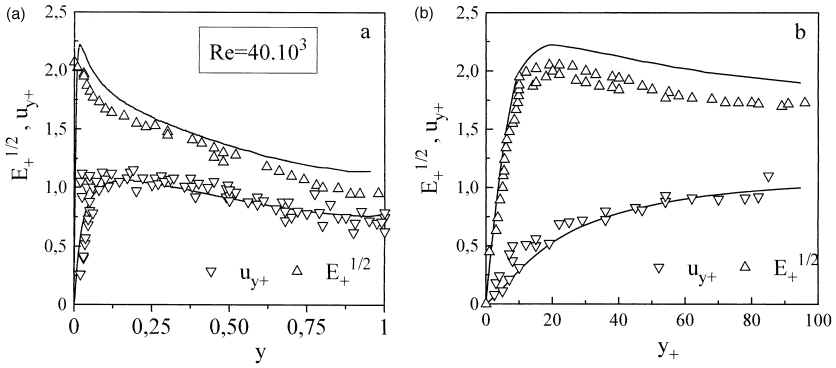


Fig. 1. Comparison between calculated results (lines) and experimental data (points) [4,7,8] for the radial profiles of turbulent r.m.s velocity and amplitude of normal velocity fluctuation near the wall (a), and in the pipe cross-section (b).

## 4. Results and discussion

In the next simulations, we consider the fully developed turbulent two-phase flow in the vertical pipe. The system of equations (13), (15) and (16) was numerically integrated using a nonuniform grid, in which the mesh is diminished as the tube wall is approached. Fig. 1(a, b) illustrates the calculated results for the turbulent energy and radial component of velocity fluctuations of the continuous phase in the tube of diameter $2R = 5 \times 10^{-2}$ m at the Reynolds number $Re = 10^4$. As observed, the approximation (17) for the radial velocity fluctuations is in satisfactory agreement with the experimental data [4,7,8].

The system of dispersed phase balance equations (1), (3), (5) and (7), complemented by closing relations and boundary conditions (9)–(12), was numerically solved using a grid with nonuniform meshes along the pipe radius. When the coordinates of mesh points in the grids for calculating the continuous phase and the dispersed phase did not coincide, the parameters of the continuous medium were approximated by a cubic splain [9]. The meshes for low inertial particles ($\tau_+ < 1$) are diminished near the wall, so as to provide at least 15 mesh points at a distance from the wall $y_+ \approx \tau_+$. For particles with high value of dynamic relaxation time ($\tau_+ \geq R_+$), the mesh points are located more uniformly along the radius. The number of grid points for both types of grids were chosen to be 80. An increase in number of grid points did not lead to a noticeable change in the calculated results.

The calculated results for the parameters of the phase of low inertial particles ($\tau_+ \ll 1$) are substantially affected by the smoothness of the amplitude of normal velocity fluctuations of the continuous phase near the wall. In near-wall region ($y_+ \leq 10$), the amplitude of turbulent velocity fluctuations normal to the surface was approximated by the analytical expression [10]

$$\langle u_{y+}^2 \rangle = B_+ \left[1 - \exp(-y_+/A_+)\right]^2, \quad B_+ \approx 0.8, \quad A_+ \approx 26$$

The turbulent particles deposition rate depends on the magnitude of radial velocity fluctuations of the dispersed phase in the near-wall region. The amplitude of the fluctuating velocity of particles close to the wall has nonmonotonical dependence on their inertia (Fig. 2). Particles with high relaxation times penetrate into the near-wall region with a nonzero fluctuating velocity. When particles dynamic relaxation time is higher than the time macroscale of turbulence in the flow core, this leads to a decrease in both the amplitude and nonhomogeneity of the dispersed phase turbulent energy over the whole cross-section. Fig. 3 shows the comparison between data obtained in the frame of direct numerical simulations by Kallio and Reeks [11] and our calculation results for radial fluctuating velocity amplitude of particles normal to the wall.

In the near-wall region, particles migrate in the direction of lower amplitude level of dispersed phase

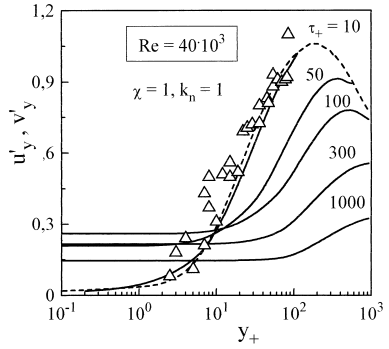


Fig. 2. Radial profiles of the particles normal velocity fluctuation amplitude with various relaxation times at the reflected elastic wall. Points are experimental data [4]. Dashed lines are amplitude of fluid velocity fluctuations, and solid lines are particles velocity fluctuations amplitude.

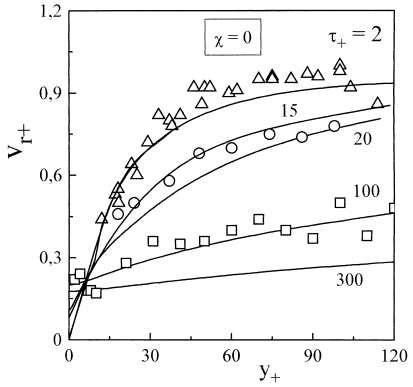


Fig. 3. Comparison between calculated results (lines) and data [11] for normal velocity fluctuations of particles with various relaxation times near the absorbing wall.

radial velocity fluctuation (turbophoresis). Fig. 4 presents, as an example, profiles of particles radial acceleration induced by gradient of turbulent energy in the near-wall region

$$A_r = \frac{1}{r}\frac{d}{dr}\left(r\langle v_r^2\rangle\right), \quad A_{r+} = A_r R/u_+^2$$

For comparison purposes in Fig. 4, the experimental results of Young and Hanratty [12] are also shown. It is seen that the acceleration of particles is directed to the pipe wall, which increases with increase in Reynolds number. A maximum of particles radial acceleration is located close to the wall.

Fig. 5(a, b) presents distribution of the turbophoretic velocity $V_{mig+} = \tau_+ A_{r+}$ and dispersed phase concentration for absorbing ($\chi = 0$) and reflecting surfaces ($\chi = 1$). The turbophoretic velocity is pointed at the wall and nonmonotonically depends on dynamic relaxation time of particles (Fig. 5(a)). Increase in the relaxation time causes increase in the turbophoretic velocity. However, for high inertial particles, the turbophoretic velocity decreases, because the profile of dispersed phase turbulent energy across the pipe becomes more flat. For elastic surface ($k_n = 1$), turbophoretic velocity on the wall is equal to zero. The maximum value for turbophoretic velocity is reached on the inelastic surface ($k_n = 0$) or absorbing wall ($\chi = 0$). The turbulent migration of particles leads to an increasing dispersed phase concentration on the reflected surface (Fig. 5(b)). Particle deposition produces reduction of the dispersed phase concentration on the absorbing surface in comparison with the reflecting surface. Increasing the particles inertia, when we obtain decreasing turbophoresis, leads to more uniform concentration profile. It should be noted that the calculated results shown in Fig. 5(b) are in satisfactory qualitative agreement with the direct numerical simulations results [3,13].

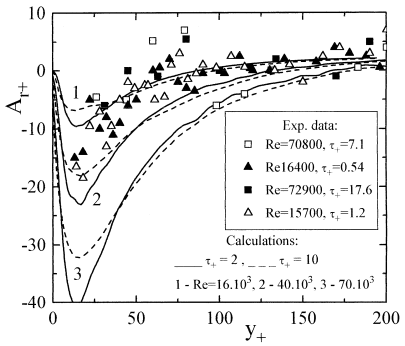


Fig. 4. Particles radial acceleration near the wall. Lines are results of calculation, and points are experimental data [12].

Fig. 6 shows the comparison between calculation results and experimental data of Liu and Agarwal [14] for particles deposition velocity. The dependence of the deposition velocity on dimensionless particles dynamic relaxation times has a maximum value. For particles with relaxation times $\tau_+ \le 10^2$, the universal growing branch, associated with particles penetration into the near-wall region, is realized. For particles with dynamic relaxation times $\tau_+ > 10^3$, the deposition velocity decreases because the amplitude of dispersed phase fluctuations is diminished. Fig. 7 illustrates particles deposition rate at various absorption coefficients $\chi$ (experimental results of Agarwal [15]). For larger Reynolds number, the maximum value of the dispersed

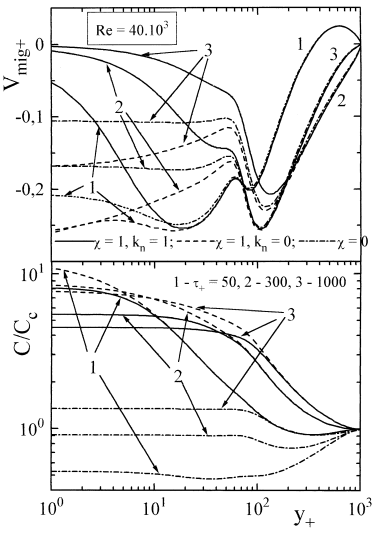


Fig. 5. Profiles of particles turbophoretic velocity (a) and dispersed phase concentration (b) at various properties of the pipe surface. Solid lines for reflected and elastic surface ($\chi = 1, k_n = 1$), dashed lines for reflected but inelastic surface ($\chi = 1, k_n = 0$), points–dashed lines for absorbing surface ($\chi = 0$).

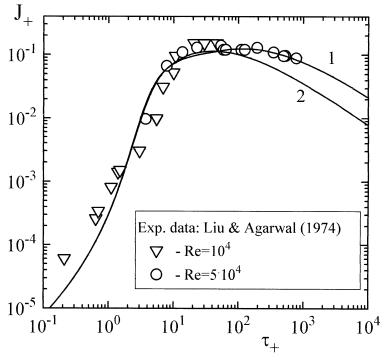


Fig. 6. Comparison of simulation results (lines) for particles deposition velocity with experimental data (points) [14]. (1) $Re = 10^4$, (2) $5 \times 10^4$.

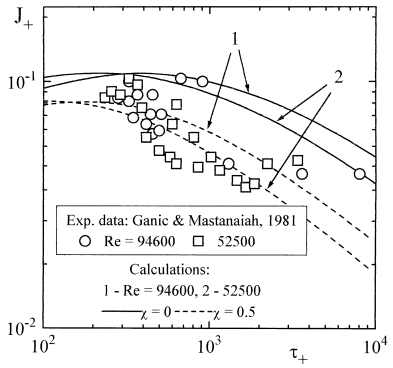


Fig. 8. Particles deposition velocity at various flow Reynolds number and absorption coefficients.

phase deposition velocity moves in the area of more inertial particles. A similar conclusion follows from our model prediction for experimental conditions of Ganic and Mastanaiah [16] (Fig. 8).

Fig. 9 presents calculated particles concentration in the pipe with absorbing wall and experimental data from Hagivara and Sato [17]. The theoretical results were obtained in the frame of "complete model" (numerical calculations with the help of Eqs. (1)–(12) and on the basis of analytical formula (23)).

Fig. 10 illustrates turbulent deposition rate of rather inertial particles $\tau_+ \geq 10^2$. The particles deposition velocity was determined with the help of the complete model and the analytical formula (24). The experimental data in Fig. 10 are collected in papers of Andreussi [18], Lee and Hanratty [19], Lee et al. [20].

Fig. 11 shows the deposition velocity in universal variables as a function of the dimensionless particles relaxation times. The experimental data in Fig. 11 was assembled in [15–17, 19–21]. For particles with $\tau_+ \leq 10^2$, the deposition rate weakly depends on absorption coefficient. For inertial particles $\tau_+ > 10^3$, the Reynolds number and the coefficient of particles absorption have notable influence on the intensity of turbulent mass transfer. The dependence of particle deposition velocity on restitution coefficient in the normal direction $k_n$ is insignificant.

Fig. 12 predicts turbulent deposition rate as a function of the flow Reynolds number. For the different sizes of particles, both growing and falling branches of deposition velocity can be realized. Flow Reynolds number augmentation induces increase in the values of dimensionless particles relaxation time. For particles with dynamic relaxation time, at the starting Reynolds number, $\tau_{min+} \leq 1$, we obtain intensification of dispersed phase mass transfer by increasing the Reynolds number. If at the minimum flow Reynolds number the particles relaxation times $\tau_{min+} \geq 10$, then growth of the Reynolds number reduces monotone deposition velocity. Fig. 12 also shows the experimental data from Papavergos and Hedley [21].

Fig. 13 presents the dispersed phase averaged velocity profiles in the pipe cross-section without particle absorption ($\chi = 1$). The experimental results in the

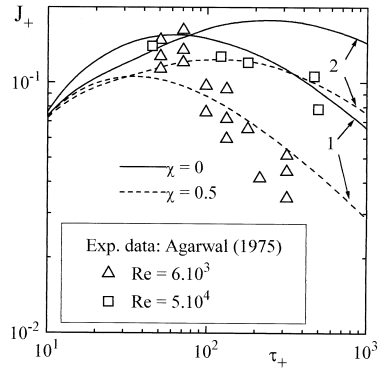


Fig. 7. Influence of the absorption coefficient on the particles deposition rate. Lines are calculated results, and points are experimental data [15]. (1) $Re = 6 \times 10^3$, (2) $5 \times 10^4$.

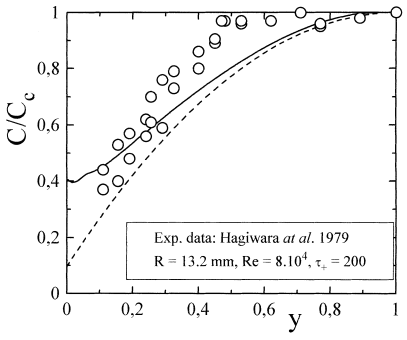


Fig. 9. Dispersed phase concentration profile obtained by the complete model (solid lines) and by the analytical formula (23) (dashed lines).

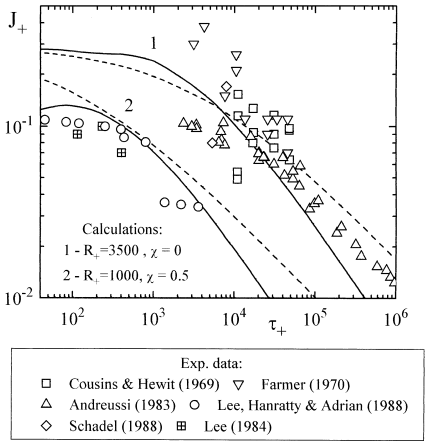


Fig. 10. Comparison between experimental data collected in [18–20] and predictions obtained by the complete model (solid lines) and by the analytical formula (24) (dashed lines).

figure belong to Lee and Durst [22]. Particles lose axial momentum after their collisions with the pipe wall, and this process determines the appreciable velocity difference between continuos and dispersed phases (Fig. 13(a)). Near the wall, dispersed phase velocity is greater than fluid velocity, but in the core region, particles velocity is lesser than the carrying phase velocity. Growth in the particles inertia and particles gravitational settling velocity elevated the velocity slip between phases.

The experiments manifest that amplitude of dispersed phase velocity fluctuations in axial direction is much higher than in radial direction. This effect is a result of the additional generation of the particles random movement in the axial direction due to a gradient of the dispersed phase average velocity. Illustration of this effect is presented in Fig. 13(b, c).

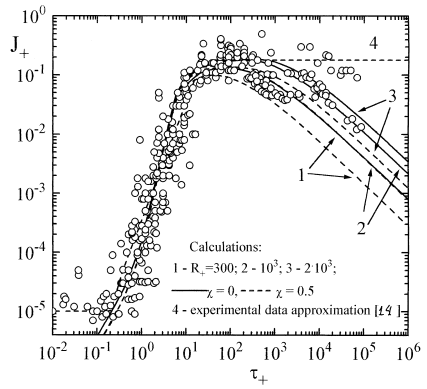


Fig. 11. Influence of Reynolds numbers and absorption coefficients on particles deposition rate. Points are experimental data accumulated in [15–17, 19–21].

Finally, we would like to note that dynamics of large particles is determined not only by viscous friction force but also by Magnus lift force, arising as a result of particles rotation around their center after collisions with a surface. This problem is not examined in the present paper.

## 5. Conclusions

On the basis of two-equation turbulence model, the closed system of the balance equations for computation of hydrodynamics and dispersed phase mass transfer in vertical pipes is developed. We investigated the volumetric concentration of particles at which it is reasonable to neglect particle–particle collisions.

The effects of particles relaxation time, turbulence nonhomogeneity, coefficients of impulse restitution and particles absorption on the particles chaotic motion intensity, dispersed phase concentration distribution, and averaged velocity slip between carrying and dispersed phase are examined.

Results of numerical modeling are summarized below:

1. With increase in particles inertia, the particles penetration in the near-wall region is realized. The energy of the particles chaotic motion near the wall exceeds the turbulent energy of the carrying phase. With further growth in particles relaxation time, the profile of the particles chaotic motion intensity is reduced and becomes more flat over the cross-section. The particles chaotic motion near the wall causes particles deposition on the wall and loss of the dispersed phase axial momentum.
2. The particles turbulent deposition velocity and profile of particles concentration are controled by tur-

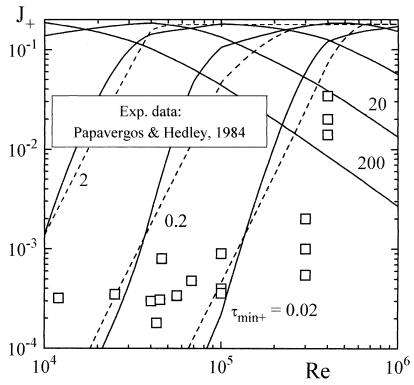


Fig. 12. Dependence of particles turbulent velocity deposition on the fluid flow Reynolds numbers. Solid lines are complete model predictions, and dashed lines are obtained by empirical approximation [14].

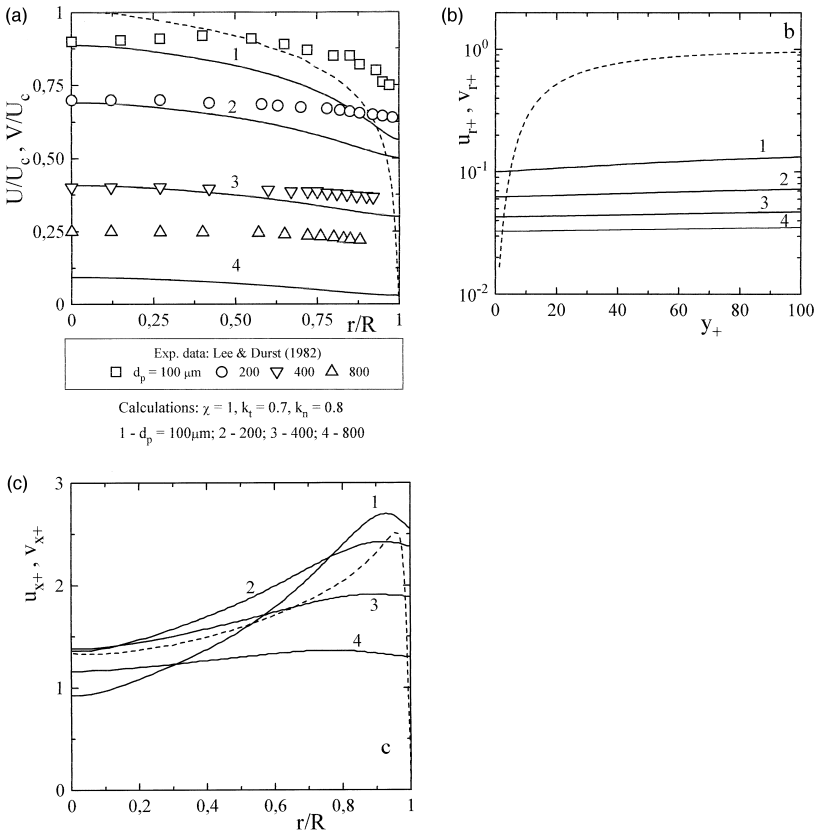


Fig. 13. Calculated results (lines) and experimental data (points) [22] for averaged axial dispersed phase velocity in the vertical pipe (a). Predictions for velocity fluctuations of dispersed phase (solid lines) and fluid (dashed lines) in radial (b) and axial (c) directions. Calculations were made at experimental conditions [22].

bophoretic velocity connected with gradient of the particles turbulent energy, and particles diffusion associated with nonuniformity of the dispersed phase concentration. For inertial particles, the role of turbophoresis is reduced, which allows us to find analytical expressions for particles deposition velocity. The intensity of turbulent mass transfer is strongly determined by the coefficient of particles absorption on the wall.

3. Amplitudes of the particles chaotic motion in axial and radial directions significantly differ from each other. Intensity of the particles chaotic motion in axial direction is much higher than in radial direction due to extra generation of the particles turbulence from the average velocity of the dispersed phase.

## Acknowledgements

This work was supported by the International Science Foundation INTAS (Grant No. 94-4348) and Russian Foundation of Fundamental Science Researches (Grant No. 98-01-00353).

## Appendix A

Balance equations for concentration and radial velocity of dispersed phase in cylindrical coordinates are

$$\frac{1}{r}\frac{\partial}{\partial r}(rCV_{\mathrm{r}}) + \frac{\partial}{\partial x}CV_{\mathrm{x}} = 0 \tag{A1}$$

$$V_{\mathrm{r}}\frac{\partial V_{\mathrm{r}}}{\partial r} + \frac{1}{r}\frac{\partial}{\partial r}\left(r\langle v_{\mathrm{r}}^2\rangle\right) = \frac{U_{\mathrm{r}} - V_{\mathrm{r}}}{\tau} - \frac{D_{\mathrm{p}}}{\tau}\frac{\partial \ln C}{\partial r} \tag{A2}$$

The approximate presentation for radial velocity of dispersed phase follows from Eq. (2) without convective term and $U_{\mathrm{r}} = 0$

$$V_{\mathrm{r}} \approx -\frac{\tau}{r}\frac{\partial}{\partial r}\left(r\langle v_{\mathrm{r}}^2\rangle\right) - D_{\mathrm{p}}\frac{\partial \ln C}{\partial r} \tag{A3}$$

After integrating Eq. (A1) over the pipe cross-section,

we obtain

$$\frac{2}{R}C_{\mathrm{w}}V_{\mathrm{rw}} = -\frac{\partial}{\partial x}(CV_{\mathrm{x}})_{\mathrm{m}},$$
$$(CV_{\mathrm{x}})_{\mathrm{m}} = \frac{2}{R}\int_0^R rCV_{\mathrm{x}}\,\mathrm{d}r \tag{A4}$$

where $V_{\mathrm{rw}} = V_{\mathrm{r}}(R)$ is radial velocity at the pipe wall.

We define particles deposition rate as

$$C_{\mathrm{w}}V_{\mathrm{rw}} = JC_{\mathrm{m}}$$

Utilizing the approximation

$$\frac{\partial}{\partial x}(CV_{\mathrm{x}})_{\mathrm{m}} \approx \frac{\partial}{\partial x}CV_{\mathrm{x}} \tag{A5}$$

we derive from Eqs. (A1) and (A4) the equation for radial velocity of dispersed phase

$$\frac{1}{r}\frac{\partial}{\partial r}(rCV_{\mathrm{r}}) = \frac{2}{R}C_{\mathrm{m}}J \tag{A6}$$

The formula (7) for radial velocity of dispersed phase is the solution of Eqs. (A6) and (A3).

## References


[1] I.V. Derevich, Statistical modelling of mass transfer in turbulent two phase dispersed flows—1. Model development, Int. J. Heat Mass Transfer 43 (2000).

[2] J. Herrero, F.X. Grau, J. Grifoll, F. Giralt, A near wall k–e formulation for high Prandtl number heat transfer, Int. J. Heat Mass Transfer 34 (3) (1991) 711–721.

[3] O. Simonen, Q. Wang, K.D. Squires, Comparison between two-fluid model predictions and large eddy simulation results in a vertical gas–solid turbulent channel flow, in: ASME Fluids Engineering Division Summer Meeting, FEDSM'97-3625, 1997, pp. 1–9.

[4] M.Kh. Ibragimov, V.P. Subbotin, V.P. Bobkov, et al., The Structure of Turbulent Flow and the Mechanism of Heat Transfer in Channels, Atomizdat, Moscow, 1978 (in Russian).

[5] H. Schlicting, Boundary Layer Theory, McGraw-Hill, New York, 1974.

[6] R.G. Boothroyd, Turbulence characteristics of the gaseous phase in duct flow of a suspension of fine particles, Trans. Inst. Chem. Ing. 45 (1967) T 297.

[7] J. Laufer, The structure of turbulence in fully developed pipe flow, NASA Technical Note 2954, 1953.

[8] G.B. Schubauer, Turbulent processes as observed in boundary layer and pipe, J. Appl. Phys. 25 (1) (1954) 188–196.

[9] G.I. Marchuk, Methods of Computational Mathematics, Nauka, Moscow, 1980.

[10] T. Cebesi, A.M.O. Smith, Analysis of Turbulent Boundary Layers, Academic Press, New York, 1974.

[11] G.A. Kallio, M.W. Reeks, A numerical simulation of particle deposition in turbulent boundary layer, Int. J. Multiphase Flow 15 (3) (1989) 433–446.

[12] J.B. Young, T.J. Hanratty, Optical studies on the turbulent motion of solid particles in a pipe flow, J. Fluid Mech. 231 (1991) 665–688.

[13] W.S.J. Uijttewaal, R.V.A. Oliemans, Particles dispersion and deposition in direct numerical and large eddy simulations of a vertical pipe flows, Phys. Fluids 8 (10) (1996) 2590–2604.

[14] B.Y.H. Liu, J.K. Agarwal, Experimental observation of aerosol deposition in turbulent flow, J. Aerosol. Sci. 5 (1) (1974) 145–155.

[15] J.K. Agarwal, Aerosol sampling and transport, Ph.D. Thesis, University of Minnesota, Particle Tech. Lab. Publ., 1975.

[16] E.M. Ganic, K. Mastanaiah, Investigation of droplet deposition from a turbulent gas stream, Int. J. Multiphase Flow 7 (2) (1981) 401–422.

[17] Y. Hagivara, T. Sato, An experimental investigation on liquid droplets diffusion in annular-mist flow, in: 2nd Multi-phase Flow and Heat Transfer Symp-Workshop, Miami, FL, 1979.

[18] P. Andreussi, Droplet transfer in two-phase annular flow, Int. J. Multiphase Flow 9 (6) (1983) 697–713.

[19] M.M. Lee, T.J. Hanratty, The inhibition of droplet deposition by the presence of a liquid wall film, Int. J. Multiphase Flow 14 (2) (1988) 129–140.

[20] M.M. Lee, T.J. Hanratty, R.J. Adrian, The interpretation of droplet deposition measurements with a diffusion model, Int. J. Multiphase Flow 15 (3) (1989) 459–469.

[21] P.G. Papavergos, A.B. Hedley, Particle deposition behaviour from turbulent flows, Chem. Eng. Res. Des. 62 (1984) 275–295.

[22] S.L. Lee, F. Durst, On the motion of particles in turbulent duct flow, Int. J. Multiphase Flow 1 (2) (1982) 125–128.